



## 1 Characterization of the Particle Emission from Ships Operating at 2 Sea Using Unmanned Aerial Vehicles

3 Tommaso F. Villa<sup>1</sup>, Reece Brown<sup>1</sup>, E. Rohan Jayaratne<sup>1</sup>, L. Felipe Gonzalez<sup>2</sup>, Lidia Morawska<sup>1</sup>, Zoran  
4 D. Ristovski<sup>1\*</sup>

5 <sup>1</sup> International Laboratory for Air Quality and Health (ILAQH), Queensland University of Technology (QUT), 2 George St,  
6 Brisbane QLD 4000

7 <sup>2</sup> Australian Research Centre for Aerospace Automation (ARCAA), Queensland University of Technology (QUT), 2 George  
8 St, Brisbane QLD 4000

9 Correspondence to: Zoran D. Ristovski (z.ristovski@qut.edu.au)

10 **Abstract.** This research demonstrates the use of an unmanned aerial vehicle (UAV) to characterize the gaseous (CO<sub>2</sub>) and  
11 particle (10 - 500 nm) emissions of a ship at sea. The field study was part of the research voyage “The Great Barrier Reef as  
12 a significant source of climatically relevant aerosol particles” on-board the RV Investigator around the Australian Great  
13 Barrier Reef. Measurements of the RV Investigator exhaust plume were carried out while the ship was operating at sea, at a  
14 steady engine load of 30%.

15 The UAV system was flown autonomously using several different programmed paths. These incorporated different altitudes  
16 and distances behind the ship in order to investigate the optimal position to capture the ship plume. Five flights were  
17 performed, providing a total of 27 horizontal transects perpendicular to the ship exhaust plume. Results show that the most  
18 appropriate altitude and distance to effectively capture the plume was 25 m above sea level and 20 m downwind.

19 Particle number (PN) emission factors (EF) were calculated in terms of number of particles emitted (#) per weight of fuel  
20 consumed (Kg fuel). Fuel consumption was calculated using the simultaneous measurements of plume CO<sub>2</sub> concentration.

21 Calculated  $EF_{PN}$  were between  $9.19 \times 10^{14}$  and  $5.15 \times 10^{15} \text{ #(Kg fuel)}^{-1}$ . These values are in line with those reported in the  
22 literature for ship emissions ranging from  $0.2$  to  $6.2 \times 10^{16} \text{ #(Kg fuel)}^{-1}$  to  $6.2 \times 10^{16} \text{ #(Kg fuel)}^{-1}$ .

23 This UAV system successfully assessed ship emissions to derive emission factors (EFs) under real world conditions. This is  
24 significant as, for the first time, it provides a reliable, inexpensive and accessible way to assess and potentially regulate ship  
25 emissions.

### 26 1. Introduction

27 Shipping is the most significant contributor to international freight, with almost 80% of the worldwide merchandise trade by  
28 volume transported by ships in 2015 (UNCTAD 2015). Emissions from this transportation mode are a significant contributor  
29 to air pollution, both locally and globally. Ships are a major pollutant source in areas surrounding harbours (Viana et al.  
30 2014), with over 70% of emissions reaching 400 km inland (Fuglestvedt et al. 2009). In 2012 exhaust from diesel engines,  
31 the predominant source of ship power, was classified as a group 1 carcinogen by the International Agency for Research on  
32 Cancer (IARC). In 2007, pollution from ship exhaust was found to be responsible for approximately 60,000  
33 cardiopulmonary and lung cancer deaths worldwide annually (Corbett et al. 2007a). Such emissions are also a strong climate  
34 forcing agent, contributing to global warming through the absorbance of solar and terrestrial radiation (Hallquist et al. 2013a;  
35 Lack et al. 2011; Winnes et al. 2016).

36 Despite these findings, emissions from shipping have consistently been subject to less regulation than those of land-based  
37 transport with ship emissions in international waters remaining one of the least regulated parts of the global transportation  
38 system (Cooper 2001; 2005; Corbett and Farrell 2002; Corbett and Koehler 2003; Eyring et al. 2005; Streets et al. 1997;  
39 USEPA-OTAC 2012). Currently, no specific restrictions for ship-emitted particulate matter (PM) exist, with the only  
40 regulated pollutants being NO<sub>x</sub> and SO<sub>2</sub>. The International Maritime Organization (IMO) recently revised the regulation of



41 these gaseous pollutants through the Annex VI of the International Convention for the Prevention of Pollution from Ships –  
42 the Marine Pollution Convention (MARPOL). The IMO expected that these regulations would lead to an indirect decrease in  
43 particle number (PN) concentration due to the reduction of NO<sub>x</sub> emissions and the use of fuel with lower sulphur content  
44 [14]. However, it has been found that the use of some low sulphur fuels lead to increased PN concentrations at lower engine  
45 loads (Anderson et al., 2015), which stresses the importance for regulation specifically addressing particulate matter (PM).  
46 The majority of emitted PM is in the ultrafine size range, < 0.1 μm, which have been demonstrated to have a particularly  
47 significant impact on health and the environment (WHO 2013). However, due to the lack in regulation, ultrafine particles, in  
48 terms of PN concentration, emitted from ships have remained unassessed in real world conditions. Quantifying PN  
49 concentration is critical to improve our understanding of shipping's impact on health and climate (Anderson et al. 2015;  
50 Blasco et al. 2014; Chen et al. 2005; Cooper 2001; Corbett and Farrell 2002; Corbett et al. 2007b; Isakson et al. 2001;  
51 Mueller et al. 2015; Reda et al. 2015; Ristovski et al. 2012; Williams et al. 2009). To achieve this, wide-scale evaluation of  
52 ship emission factors (EFs) is necessary. EFs are commonly expressed as the amount of pollutant (x) emitted per unit mass  
53 of fuel consumed g(x). (Kg fuel)<sup>-1</sup>. Different methods have been used to investigate ship EFs, including laboratory test-bench  
54 studies, on-board measurements, and measurement of ship emission plumes.  
55 Test-bench studies (Anderson et al. 2015; Kasper et al. 2007; Mueller et al. 2015; Petzold et al. 2008; Petzold et al. 2010;  
56 Reda et al. 2015) have been used to characterize emissions from different engines at various loads in laboratory conditions.  
57 However, engine performance and emissions have been shown to be different in real world operations when compared to  
58 laboratory studies. This calls for measurements of ship emissions in-situ to collect reliable data for EF calculations (Agrawal  
59 et al. 2008; Blasco et al. 2014; Murphy et al. 2009). To date, only a few studies have been undertaken on-board ships to  
60 calculate real emission factors (Hallquist et al. 2013b; Juwono et al. 2013). This is attributed to the prohibitive costs and time  
61 commitments of setting up and maintaining on-board measurement equipment on commercial ships. Airborne ship plume  
62 measurements (Balzani Lööv et al. 2014; Beecken et al. 2014a; Berg et al. 2012; Cappa et al. 2014; Lack et al. 2008; Lack et  
63 al. 2009; Pirjola et al. 2014a; Schreier et al. 2015; Sinha et al. 2003; Westerlund et al. 2015) offer an alternative method of  
64 in-situ measurements without requiring on-board monitoring stations. In the past the cost, the significant difficulties in  
65 deployment of these systems, and the risk for manned aircrafts have limited their feasibility. However, this has recently  
66 changed with the rapid advances being made in commercially available Unmanned Aerial Vehicle (UAV) technology.  
67 Hexacopter UAVs have seen a wide scale increase in industry and research applications due to their ease of use and  
68 comparatively low cost (Brady et al. 2016; Gonzalez et al. 2011; Malaver Rojas et al. 2015). Used in conjunction with air  
69 monitoring equipment, these systems provide, for the first time, the ability to perform relatively simplistic and cost-effective  
70 airborne measurements of ship emissions. However, to date no studies have reported the use of a UAV system capable of  
71 collecting data to calculate the EF of PN concentration for ships at sea.  
72 This research utilized a customized hexacopter UAV carrying instruments for PN concentration and CO<sub>2</sub> measurements to  
73 derive EF<sub>PN</sub>. The UAV system was deployed from the RV Investigator research vessel while at sea. Autonomous  
74 measurements of the RV investigators exhaust plume were taken over several flights at various altitudes and distances from  
75 the ship. Data collected was used to optimize the sampling flight path and successfully quantify the RV investigators EF for  
76 PN concentration.

## 77 2. Methodology and Measurement system

78 Measurements were conducted as part of the research voyage “The Great Barrier Reef” as a significant source of climatically  
79 relevant aerosol particles” aboard the RV Investigator research vessel over a two day period of the 13 and 14 October 2016  
80 (day 1 and day 2). Measurements of PN and CO<sub>2</sub> concentration emitted by the RV Investigator were taken using a PN and  
81 CO<sub>2</sub> monitor mounted on a customized DJI EVO S800 hexacopter UAV (DJI 2014).



82 **2.1. The RV Investigator and the voyage**

83 The RV Investigator is a sophisticated ocean research vessel configured to enable a wide range of world class atmospheric,  
84 biological, goescience and oceanographic research. The vessel is 94 m long, has a gross weight of 6,082 tons, a fuel capacity  
85 of 700 tons of ultra-low sulphur diesel fuel. It is powered by three 9 cylinder 3000 kW MaK diesel engines, each coupled to  
86 a 690V AC Generator. Ship propulsion is achieved using two 2600 kW L3 AC reversible propulsion motors powered by  
87 these generators. The RV Investigator can host up to 30 crew members and 35 researchers for a maximum voyage period of  
88 60 days with at a maximum cruising speed of 12 knots.

89 A suite of instrumentation for atmospheric research is available on the RV Investigator. This includes a radar system capable  
90 of collecting weather information within a 150 km radius of the vessel, and instruments measuring: sunlight parameters;  
91 aerosol composition, particle concentration and size distributions; cloud condensation nuclei; gas concentrations; and various  
92 other components of the atmosphere. These instruments are housed inside two dedicated on-board laboratories for aerosol  
93 and for atmospheric chemistry research. An atmospheric aerosol sample is continuously drawn into the laboratories for  
94 analysis through a specialized inlet fitted to the foremast of the ship. Of particular interest to this study, the ship contains a  
95 PICARRO (PICARRO Inc., Santa Clara, California, USA) G2401 analyser (Inc. 2017) that continuously measures CO<sub>2</sub>, CO,  
96 H<sub>2</sub>O and CH<sub>4</sub>. It has an operation range between 0-1000 ppm and a parts-per-billion sensitivity (ppb) for CO<sub>2</sub>.

97 The two day UAV measurement study was possible as part of the RV Investigator voyage “The Great Barrier Reef as a  
98 significant source of climatically relevant aerosol particles”, which started in Brisbane on the 28<sup>th</sup> of September 2016. The  
99 ship was used as both: a floating platform to allow launch and recovery of the UAV system; and as the source of an exhaust  
100 plume measured by the UAV system for EF calculation. During a several day stationary period on the Great Barrier Reef off  
101 the coast of Australia, it was possible to measure the ship plume under stable real world conditions over two consecutive  
102 days. One of the three ship engines was maintained at a steady engine load of 25 – 30 % of the maximum engine power  
103 during all measurements.

104 **2.2. UAV system**

105 Measurements of PN and CO<sub>2</sub> concentrations in the ship plume were performed using two commercial sensors mounted on-  
106 board a hexacopter UAV. The UAV used (Figure 1) is a composite material S800 EVO manufactured by DJI (DJI 2014).  
107 The UAV is 800 mm wide and 320 mm in height, with an unloaded weight of 3.7 kg. Minimum and maximum take-off  
108 weights are 6.7 kg and 8 kg, respectively. The UAV contains a 16000 mAh LiPo 6 cell battery, which provides a hover time  
109 of approximately 20 min when operating at minimum take-off weight. The telemetry range of the UAV is 2 km, which was  
110 adequate to cover the desired sampling area (See Figure 2).

111 The payload consisted of a PN concentration and a CO<sub>2</sub> monitor mounted on-board underneath the UAV. Careful placement  
112 of the payload was required to prevent flight issues caused by an altered centre of gravity. Also included was a carbon fibre  
113 rod, which extended outward horizontally from the UAV. The sampling lines for the monitors were attached to the end of  
114 this rod to ensure that measurements were not affected by the downwash of the UAV rotors. The total weight of the payload  
115 was (1.2 kg), which allowed the UAV system to fly for 12-15 min before landing at the home point (A) (See Figure 2).

116 The S800 was used in conjunction with the DJI Wookong autopilot. The software provides an intuitive and easy to use  
117 interface where autonomous flight paths can be planned, saved, and uploaded into the UAV. In addition to this, the ground  
118 station allows for continuous, real-time monitoring of the status of the UAV during operation; which includes its longitude,  
119 latitude, altitude, waypoint tolerance and airspeed.

120 The DJI S800 was chosen for this study because it is designed to operate under the 20 kg all up weight (A UW) class of  
121 UAV. This reduces operational costs and avoid subjection to the tighter regulations of larger platforms. Small UAV cannot  
122 be operated above any person, or closer than 30 m of populated areas, houses and people. Furthermore, current Civil  
123 Aviation Safety Australia (CASA) regulations restrict the use of small UAV (2 and 20 kg) to visual line-of-sight daylight



124 operation, with a maximum altitude of approximately 120 m and within a radius of 3 nmi of an airport. UAVs in this  
125 category are not permitted for research unless the research institution has been granted a permit exception. These exceptions  
126 can be granted if the institution in question has or collaborates with an UAV operation team who must have: an experienced  
127 UAV pilot who is also radio controller specialist; a license for commercial UAV operation; and appropriate liability  
128 insurance. Queensland University of Technology (QUT) has an unmanned operator certificate and four pilots who have  
129 UAV controller licenses.

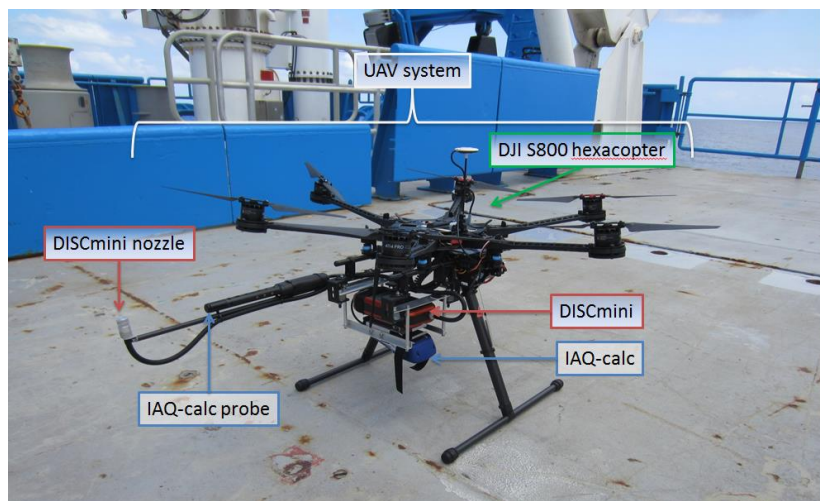
130 **2.2.1. Instrumentation**

131 **2.2.1.1. Instrumentation for PN concentration**

132 This study measured PN concentration using a Mini Diffusion Size Classifier (DISCmini), developed by the University of  
133 Applied Sciences, Windisch, Switzerland (Fierz et al. 2008). The DISCmini is a portable monitor used to measure  
134 concentration of particles in the 10-500 nm diameter size range, with a time resolution of up to 1s (1 Hz). It can measure PN  
135 concentrations between  $10^3$  and  $10^6$  N/cm<sup>3</sup>. Measurement accuracy is dependent upon the particle shape, size distribution,  
136 and number concentration. The advantages of using the DISCmini are its relatively small dimensions (180 x 90 x 40 mm),  
137 low weight (640 g, 780 g with the sampling probe, Figure 1) and long battery life of up to 8 hrs. These  
138 characteristics allow it to be easily integrated on the UAV.

139 **2.2.1.2. Instrumentation for CO<sub>2</sub> concentration measurements**

140 A TSI (TSI, Shoreview, Minnesota, United States) IAQ-calc 7545 model was chosen to measure CO<sub>2</sub> concentrations. Its  
141 sensor is based on a dual-wavelength NDIR (non-dispersive infrared) with a sensitivity range between 0 to 5,000 ppm and an  
142 accuracy of  $\pm 3.0\%$  of reading or  $\pm 50$  ppm (whichever is greater). The measurement resolution is 1 ppm with a maximum  
143 time resolution of 1s. Similar to the DISCmini, the advantages of using the IAQ-calc are: its small dimensions (178 x 84 x 44  
144 mm); low weight (270 g, with batteries, significantly lower than the DISCmini), and a battery life of 10 hours.  
145 The readings of the IAQ-calc for CO<sub>2</sub> were compared with those measured by the on-board PICARRO G2401 analyser.  
146 Both the DISCmini and the IAQ-calc were tested and calibrated in the laboratory prior to the commencement of the  
147 measurements (Figure S1 in the Supplementary Material). All data was logged with a 1 s time interval.



148

149 **Figure 1. The UAV system with the on-board instrumentation: the DISCmini and the IAQ-calc.**

150



151 **2.3. Meteorological data**

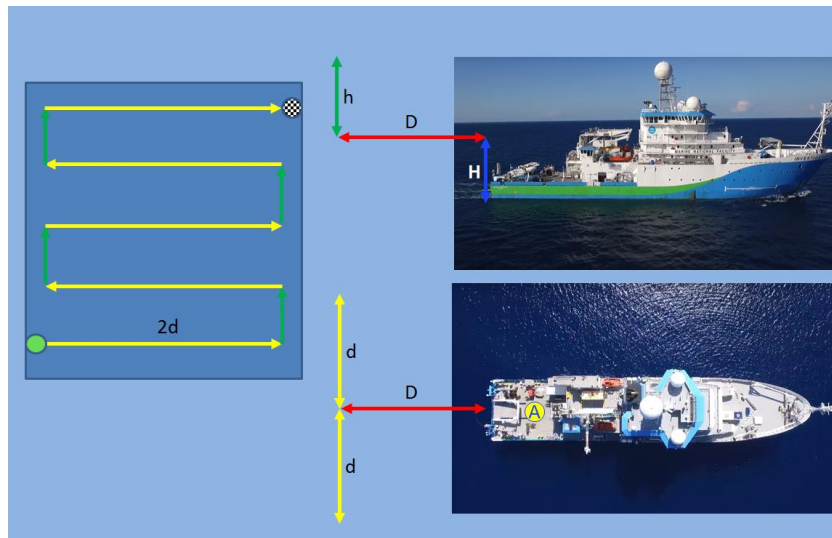
152 Meteorological data (including air temperature, relative humidity, atmospheric pressure, wind speed and direction) were  
153 recorded by the RV Investigators on-board instrumentation during the entire voyage with a 60 s time interval, 24/h a day.

154 **2.4. Study design**

155 During the two measurement days of this study, the vessel was heading into the wind whilst idling the UAV missions at sea.  
156 This positioning caused the exhaust plume to extend downwind, directly behind the ship. The UAV system was launched off  
157 the back deck, autonomously sampling at varying altitudes and distances into the downwind plume. Flight speed of the UAV  
158 was 1.5 m/s, the minimum for the S800.

159 Day 1 was used to optimise the study design, focusing on finding the flight path most suitable to capture the ship plume.  
160 Figure 2 shows the programmed flight path, which consisted of a continuous flight beginning at a distance (D) and from an  
161 altitude (H) above the surface. Point A, located on the back deck of the RV Investigator, represents the 'home point'. In  
162 UAV terminology this refers to the position where the UAV system takes off and lands. The UAV system was programmed  
163 to move horizontally by a distance (2d), perpendicular to the ship, then climb vertically for 10 m (h) before flying in the  
164 opposite horizontal direction for the same distance (2d). The UAV was then programmed to climb another 10 m (h) before  
165 repeating this pattern until the UAV reached an altitude of 65 m above the ocean. During day 1, the UAV system followed  
166 three different flight paths, each one with both a different distance D behind the ship (20, 50 and 100 m), and a different  
167 horizontal distance 2d (50, 100 and 150 m).

168 The optimised flight path for day 2 started 20 m behind the ship and 25 m above the surface, with no altitude variation. The  
169 UAV path was limited to a continuous horizontal flight of 50 m (2d) at steady speed of  $2 \text{ m s}^{-1}$ . This path and flying speed  
170 allowed up to 4 horizontal transects to capture the ship plume.



171

172 **Figure 2. Flight path used to capture the plume: H - height from the ocean, D – distance behind the ship to the flight beginning**  
173 **point, h – rising altitude after the horizontal transect, 2d – full length of the horizontal transect**

174 **2.5. Experimental procedure**

175 The UAV can fly either manually or autonomously. As a safety precaution, every take-off and landing was performed using  
176 the manual flight mode. Once in the air, the UAV was switched to autonomous flight mode, allowing the platform to follow  
177 the pre-programmed flight path discussed in the previous section. The flight path consisted of waypoints, which are three-



178 dimensional GPS points that dictate the position of the UAV along the flight path. The waypoints and flight plans for each  
179 flight were programmed using the aforementioned DJI Wookong ground station software. The DISCmini and the IAQ-calc  
180 were fitted on the underside of the UAV at the beginning of each measuring day. Five flights were performed across the two  
181 measurement days, providing a total of 27 horizontal transects perpendicular to the ship's exhaust plume.

182 **2.6. Emission factors**

183 The calculation of an emission factor for particle number concentration ( $EF_{PN}$ ) from the collected ship plume measurements  
184 was performed using Eq. (1). This method has previously been used for ship (Westerlund et al. 2015), road vehicle (Hak et  
185 al. 2009) and aircraft (Mazaheri et al. 2009) emissions. The measured values of PN concentration were related to the amount  
186 of fuel consumed by the engine in question through the use of the simultaneous measurements of CO<sub>2</sub> concentration taken by  
187 the UAV. This was achieved by using a published value for a ship emission factor of CO<sub>2</sub> ( $EF_{gas}$ ) of 3.2 Kg CO<sub>2</sub> (Kg fuel)<sup>-1</sup>  
188 (Hallquist et al. 2013b; Hobbs et al. 2000) .

189 Eq.(1).

$$190 \quad EF_{PN} = \frac{\Delta PN}{\Delta gas} \times EF_{gas} \quad (1)$$

191 The  $\Delta PN$  and  $\Delta gas$  in Eq. (1) represent changes in the measured particle number and CO<sub>2</sub> concentrations, respectively.  
192 Background concentrations of PN and CO<sub>2</sub> were subtracted and  $EF_{PN}$  was calculated by integrating the peak plume  
193 concentration measured by the DISCmini and IAQ-clac mounted on the UAV system; which is defined as the average  
194 concentration measured by the DISCmini and IAQ-calc outside the ship plume.

195

196 **3. Results and Discussion**

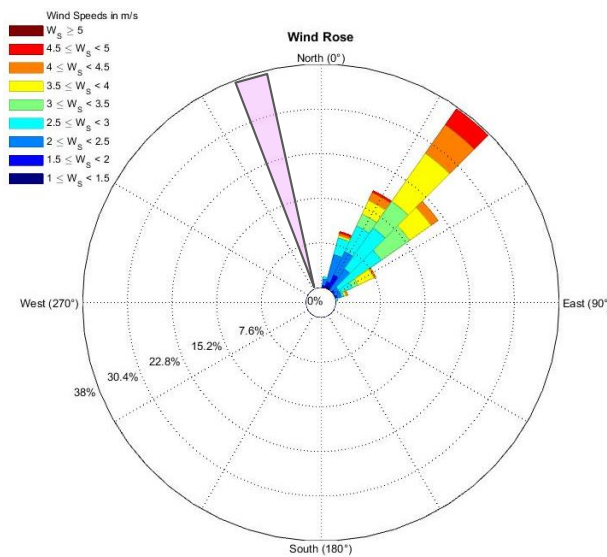
197 **3.1. Meteorological and Investigator data**

198 Wind conditions were very stable during both day 1 and day 2, following one main pattern for the entire flight time. The  
199 wind speed ranged from 3 - 13 m s<sup>-1</sup>. The wind direction was predominantly from the NE during day 1 and ESE during day  
200 2.

201 The wind rose graphs in Figure 3a and 3b illustrate the wind data recorded with the on-board weather instrumentation during  
202 all horizontal transects flown during day 1 and 2 respectively. The prevalent wind direction was ESE, which corresponded to  
203 the heading of the RV Investigator (indicated by the rose triangle).

204 The wind direction changed occasionally to E during the flight, causing the UAV to fail to capture the RV Investigator  
205 plume during some transects. As a result, 2 of the 8 horizontal transects collected on day 2 were excluded from the analysis.

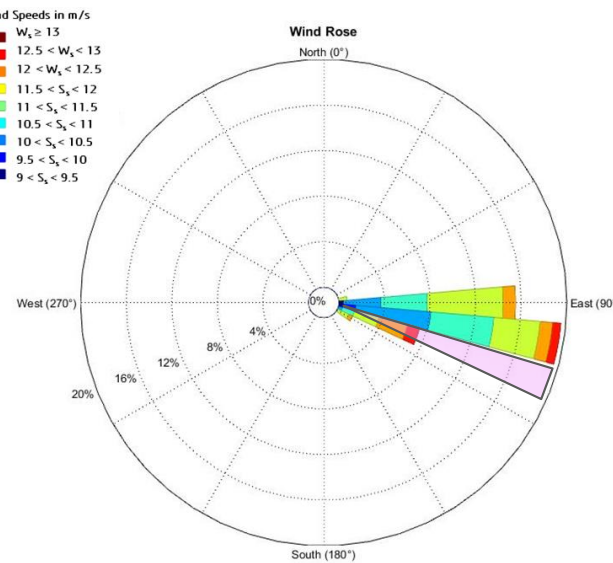
206



207

208 **Figure 3a – Wind rose showing wind speed and direction during day 1. Rose triangle shows RV Investigator direction during the**  
 209 **measurements.**

210



211

212 **Figure 3b – Wind rose showing wind speed and direction during day 2 optimized flight. Rose triangle shows RV Investigator**  
 213 **direction during the measurements.**

### 214 **3.2. UAV system horizontal transects inside and outside the plume**

215 The UAV system acquired data for a total of 27 horizontal transects for day 1 and day 2. Data was collected at altitudes  
 216 between 25 m and 65 m above the water surface. During day 1 the plume was captured once when the UAV was at 25 m



217 altitude and 20 m downwind of the ship; and again at both 25 and 35 m altitude 100 m downwind of the ship. These  
218 observations lead to the optimized flight used on day 2, which started downwind at 25 m above the surface and 20 m behind  
219 the ship. On day 2 the UAV system successfully captured the plume during 6 of the 8 transects performed. Across the two  
220 days this lead to a total of 9 transects that captured the plume and which have been considered for discussion, shown in  
221 Table 1.

222

| Measuring day | Altitude | Distance behind the Investigator | Number of transects |
|---------------|----------|----------------------------------|---------------------|
| Day 1         | 25 m     | 20 m                             | 1                   |
| *Day 1        | 25 m     | 100 m                            | 1                   |
| Day 1         | 35 m     | 100 m                            | 1                   |
| Day 2         | 25 m     | 20 m                             | 6                   |

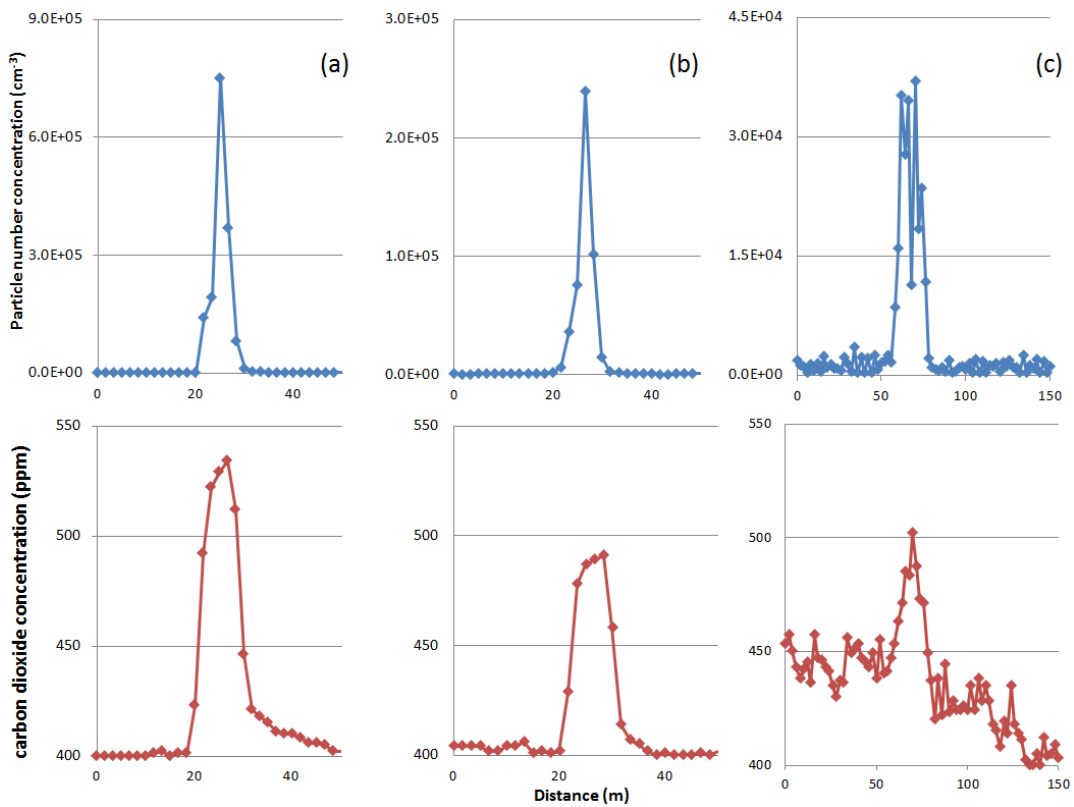
223  
224 **Table 1 – Specifications of the transects considered for the data analysis. The (\*) indicates the transect of Day 1 of which PN  
225 concentration and CO<sub>2</sub> profiles are presented in Figure 4.**

226

227 Figure 4 shows the PN concentration and CO<sub>2</sub> profiles, collected during two (a; b) transects on day 2, and (c) during one  
228 transect of day 1 (Spec. in Table 1, Day1\*).

229 The PN concentration profiles for the (a) and (b) transects in Figure 4 show that the concentration varied by five orders of  
230 magnitude between the outside and inside the plume, while the CO<sub>2</sub> profiles show an increase up to 140 ppm above the  
231 background.

232 The profiles in (c) show that the PN concentration was four orders of magnitude greater inside the plume at 100 m behind the  
233 ship and that the CO<sub>2</sub> concentration was up to 100 ppm higher inside the plume.



234

235 **Figure 4 – (a) and (b) show the PN concentration and CO<sub>2</sub> profiles collected at 20 m behind the ship 25 m above the surface during**  
236 **one of the flight in day 2. (c) shows the PN concentration and CO<sub>2</sub> profiles collected during flight 3 of day 1 at 100 m behind the**  
237 **ship, 25 m above the surface.**

238

239 Figure 4 (a) and (b) both show transects at 25 m altitude and 20 m behind the ship. Both the PN concentration and CO<sub>2</sub>  
240 measurements show clear, single peaks as the UAV crosses the plume. However, the maximum PN concentrations measured  
241 in (a) ( $7.5 \times 10^5 \text{ #.cm}^{-3}$ ) are approximately three times greater than those in (b) ( $2.4 \times 10^5 \text{ #.cm}^{-3}$ ). Furthermore, the CO<sub>2</sub>  
242 measurements between (a) and (b) have a difference of (43 ppm). As the ship engine remained under steady load throughout  
243 these measurements, the variations between (a) and (b) can be attributed to several factors which reduce the effectiveness of  
244 the UAV transect for capturing the plume. Slight changes in ambient conditions such as temperature, wind direction and  
245 intensity will alter the path of the plume as it moves away from the ship. The UAVs automated flight path cannot account for  
246 these variations. Therefore, the degree to which the UAV enters the plume, and thus the concentrations it measures, will be  
247 different on each transect. Both CO<sub>2</sub> and PN concentration measurements will be similarly affected by this variance.  
248 However; it is expected that this will contribute to the calculated error margin of the final result.

249 In comparison to Figure 4 (a) and (b), the graphs in (c) show substantially less defined, wider peaks with lower pollutant  
250 concentrations. This is attributed to a difference in flight paths, with Figure (c) representing data from a transect 100 m  
251 behind the ship; whilst (a) and (b) were performed 20 m behind the ship. As the plume travels away from the ship it will  
252 begin to turbulently mix with the surrounding air mass; causing concentrations to decrease and the plume to broaden as the  
253 pollutants spread into the atmosphere.



254 A potential benefit of the 100 m transect is that it provides more data points inside the plume when compared to the 20 m  
255 transect. However, there are clear variations in the measurements across the plume, indicating that the plume was not  
256 homogenous at this distance. This could be due to localized perturbations in the wind causing inconsistent mixing with the  
257 surrounding air mass. Furthermore, the CO<sub>2</sub> measurements do not follow the PN concentration measurements; with the peak  
258 being significantly broader and not returning to its expected background value of around 400 ppm. These issues indicate that  
259 more distant measurements, whilst providing more data points, potentially provide less accurate data for the calculation of  
260 emission factors. More accurate transect measurements could be achieved by slowing the UAV flight speed for transects  
261 closer to the emission source. However, this was not possible in this study as the S800 hexacopter UAV was flown at its  
262 minimum speed of 1.5 m/s during all transects.

### 263 3.3. PN Emission Factors

264  $EF_{PN}$  values were calculated relative to the fuel consumption using the fuel combustion derived plume CO<sub>2</sub>, (Eq. 1) and the  
265 data from the nine transects listed in Table 1.

266  $\Delta PN$  was calculated by integrating the peak plume concentration (average of five data points) measured by the DISCmini,  
267 after subtraction of the background concentration. Background concentration is defined as the concentration (average of five  
268 data points) measured outside the plume. The same calculation was made to obtain the  $\Delta CO_2$ .

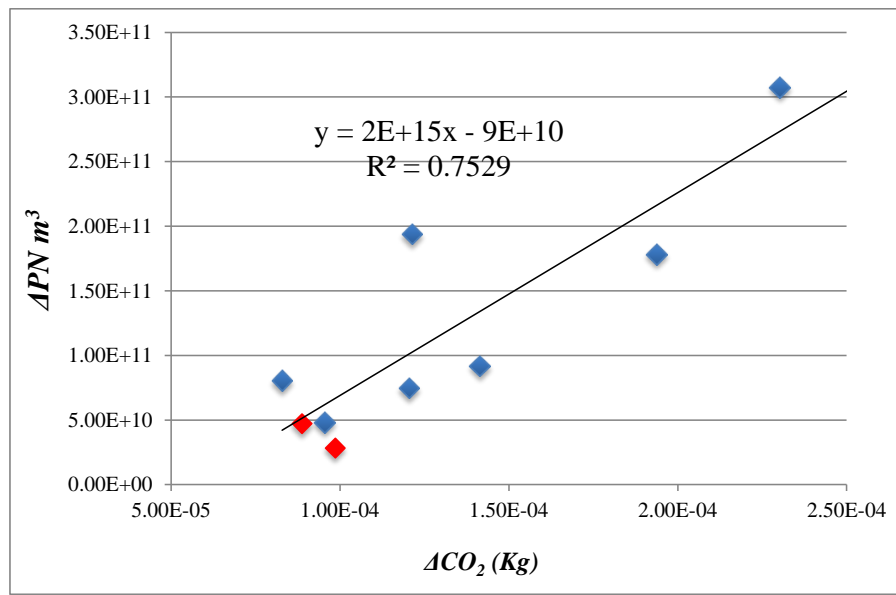
269 Table 2 shows, for each of the 9 transects, where the plume was captured, the measured concentration values of  $\Delta PN$   
270 and  $\Delta CO_2$ , in Kg per cubic meter, and the calculated  $EF_{PN}$ .

| Day | Plume captured<br>(distance and<br>altitude) | $\Delta PN \text{ m}^3$ | $\Delta CO_2 \text{ (Kg)}$ | $EF_{PN}$             |
|-----|--|-------------------------|----------------------------|-----------------------|
| 1   | 20 m; 25 m                                   | $1.94 \times 10^{11}$   | $1.21 \times 10^{-4}$      | $5.11 \times 10^{15}$ |
|     | 100 m; 25 m                                  | $2.83 \times 10^{10}$   | $9.86 \times 10^{-5}$      | $9.19 \times 10^{14}$ |
|     | 100 m; 35 m                                  | $4.72 \times 10^{10}$   | $8.88 \times 10^{-5}$      | $1.70 \times 10^{15}$ |
| 2   | 20 m; 25 m                                   | $3.07 \times 10^{11}$   | $2.30 \times 10^{-4}$      | $4.27 \times 10^{15}$ |
|     | 20 m; 25 m                                   | $9.18 \times 10^{10}$   | $1.41 \times 10^{-4}$      | $2.08 \times 10^{15}$ |
|     | 20 m; 25 m                                   | $4.81 \times 10^{10}$   | $9.55 \times 10^{-5}$      | $1.61 \times 10^{15}$ |
|     | 20 m; 25 m                                   | $1.78 \times 10^{11}$   | $1.94 \times 10^{-4}$      | $2.94 \times 10^{15}$ |
|     | 20 m; 25 m                                   | $8.05 \times 10^{10}$   | $8.29 \times 10^{-5}$      | $3.11 \times 10^{15}$ |
|     | 20 m; 25 m                                   | $7.46 \times 10^{10}$   | $1.21 \times 10^{-4}$      | $1.98 \times 10^{15}$ |

271 272 **Table 2 –  $\Delta PN$  and  $\Delta CO_2$  concentration emission/rate of the RV Investigator and calculated Emission Factors for PN.**

273

274 The  $\Delta PN$  and  $\Delta CO_2$  values were plotted and correlated against each other as shown in Figure 5.  $\Delta PN$  and  $\Delta CO_2$  were found  
275 to have a good linear relationship with an  $R^2$  value of 0.7529.



276

277 **Figure 5**  $-\Delta PN$  and  $\Delta CO_2$  for the nine transects considered for the data analysis. Red markers indicate the measurements taken at  
 278 100 m behind the ship.

279

280 The calculated  $EF_{PN}$  values for the RV Investigator ranged from  $9.19 \times 10^{14}$  to  $5.11 \times 10^{15} \# \cdot (\text{Kg fuel})^{-1}$ . The two 100 meter  
 281 transects provided the lowest two emission factors measured ( $9.19 \times 10^{14} \# \cdot (\text{Kg fuel})^{-1}$  and  $1.70 \times 10^{15} \# \cdot (\text{Kg fuel})^{-1}$ ). This is  
 282 likely a consequence of the noted differences between the plume measurements of the 20 and 100 m transects. The clear  
 283 distinction between the background and the plume measurements of the 20 m transect indicate that the  $EF_{PN}$  calculated using  
 284 them will be more representative of the RV Investigator emissions at 30% engine load. Therefore, the 100 m transects were  
 285 discounted from the calculation of the mean  $EF_{PN}$  and the corresponding standard error. These values were calculated as  $3.0 \times 10^{15} \pm 0.5 \times 10^{15} \# \cdot (\text{Kg fuel})^{-1}$ . As presented in Table 3, this value is comparable with those reported in the literature for  
 286 cruise and cargo ship plumes; which range from  $0.2 \times 10^{16}$  to  $6.2 \times 10^{16} \# \cdot (\text{Kg fuel})^{-1}$  (Alföldy et al. 2013; Beecken et al.  
 287 2014b; Jonsson et al. 2011; Juwono et al. 2013; Lack et al. 2011; Pirjola et al. 2014b; Sinha et al. 2003; Westerlund et al.  
 288 2015).

289 The calculated  $EF_{PN}$  for the Investigator were lower compared to those reported by Beecken et al. (Beecken et al. 2014a) for  
 290 passenger ships while accelerating ( $0.91 \pm 0.18 \times 10^{16} \# \cdot (\text{Kg fuel})^{-1}$ ). However, the RV Investigator measurements were  
 291 undertaken whilst its engine was under 30% load. Accelerating ships will typically be under higher engine loads and hence  
 292 have a correspondingly higher  $EF_{PN}$  (Westerlund et al. 2015), which explains part of this discrepancy. Furthermore, the RV  
 293 Investigator is a sophisticated modern vessel built for use in regions such as Antarctica. As such, it is design to have high  
 294 efficiency engines, a diesel-electric energy generation system, and uses refined, ultra-low sulphur diesel fuel. These factors  
 295 lead to the RV Investigator being more efficient and less polluting than most other ships at sea. This explains why the results  
 296 of this study are comparable to the lower end of those found in the literature.

297 The RV investigator also uses low sulphur content diesel fuel which is similar in quality to the fuels used in the ground  
 298 transport industry. In fact, the results presented here were comparable to those for in-land transportation, ranging from  $4.8 \times 10^{14}$  (25% engine load) to  $7.2$  (100% engine load)  $\times 10^{15} \# \cdot (\text{Kg fuel})^{-1}$  (Jayaratne et al. 2009). The calculated values for the



301 RV Investigators  $EF_{PN}$  are also close to data for commercial aircrafts during landing and taxiing, which range from 4.16 to  
302  $7.74 \pm 1.46 \times 10^{15} \text{ # (Kg fuel)}^{-1}$  (Mazaheri et al. 2009).

| Reference                | Measuring Platform      | EF (PN)                        | Number of ships | Location             |
|--------------------------|-------------------------|--------------------------------|-----------------|----------------------|
| This Study               | Unmanned Aerial Vehicle | $0.3 \times 10^{16}$           | 1               | Open water           |
| Westerlund et al. (2015) | Land based              | $2.35 \pm 0.20 \times 10^{16}$ | 154             | Harbor, Ship Channel |
| Beecken et al. (2014)    | Airborne                | $1.8 \pm 1.3 \times 10^{16}$   | 174             | Open water           |
| Pirjola et al. (2014)    | Land based              | $0.32 \times 10^{16}$          | 11              | Harbor, Ship Channel |
| Alföldy et al. (2013)    | Land based              | $0.8 \times 10^{16}$           | 497             | Harbor               |
| Juwono et al. (2012)     | On board                | $0.22 \times 10^{16}$          | 2               | Harbor, Ship Channel |
| Jonsson et al. (2011)    | Land based              | $2.55 \pm 0.11 \times 10^{16}$ | 734             | Harbor               |
| Lack et al. (2011)       | Airborne                | $1.0 \pm 0.2 \times 10^{16}$   | 1               | Open water           |
| Sinha et al. (2003)      | Airborne                | $6.2 \pm 0.6 \times 10^{16}$   | 2               | Open water           |

303  
304 Table 3 – Comparison of the Emission Factor for the RV Investigator found in this study with other relevant values found in  
305 literature.

#### 306 4. Summary and conclusion

307 The UAV system used in this study successfully measured PN and CO<sub>2</sub> concentrations from the exhaust plume of the RV  
308 Investigator whilst operating at sea. Several different flight paths were tested and an optimal transect flying perpendicular to  
309 the plume at a distance of 20 meters from the ship was adopted. The  $EF_{PN}$  calculated for the RV investigator ranged from  
310  $9.19 \times 10^{14}$  to  $5.11 \times 10^{15} \text{ #.(Kg fuel)}^{-1}$  relative to both consumed fuel and engine load. This  $EF_{PN}$  was within the lower end  
311 of values reported in literature, thus validating the novel UAV system for this application.

312 In comparison with other methods, the UAV system presented provides a cost effective and accessible solution for the rapid  
313 measurement and quantification of ship emissions. Its ability for deployment both in harbour and at sea, coupled with the  
314 possibility of altering its flight path to account for variances in wind conditions; gives this UAV system a distinct advantage  
315 over ground based and manned aerial vehicles. Furthermore, the UAV can sample considerably closer to the plume emission  
316 source than other methodologies, providing more accurate measurements for the calculation of  $EF_{PN}$ .

317 These attributes indicate that this UAV system provides a basis for wide-scale quantification of ultrafine particle emission  
318 factors from commercial shipping. This is critical to improve our understanding of shipping's impact on climate and health.  
319 Furthermore, it will both inform regulatory bodies, and provide them with the tools to monitor emissions in harbours and at  
320 sea.

#### 321 4.1. Recommendations

322 The possibilities of this UAV system extend far beyond what is described here. This study is intended as both: a proof of  
323 concept; and to provide useful information both for the future of this project, as well as any other UAV sampling systems



324 being developed. The instruments on-board this system were used for the measurement of PN and CO<sub>2</sub> concentrations in  
325 order to calculate  $EF_{PN}$ . However, this methodology could also be expanded to measure other important ship emission  
326 factors, including NO<sub>x</sub> and volatile organic compounds (VOCs).  
327 Further possibilities and potential improvements can also be made to the plume transect sampling method used here. The  
328 sampling error could be reduced by collecting more data points inside of the plume. One method to achieve this would be to  
329 find an optimal transect distance which provides the broadest plume cross-section, whilst also providing a clear  
330 differentiation between plume and the surrounding air mass. An alternative approach would be the use of a different UAV  
331 with a lower minimum operational speed to increase the time of the plume transect. Other study possibilities include:  
332 comparisons between  $EF_{PN}$  for different loads both in the harbour and at sea, and investigations into the use of a single flight  
333 to transect multiple ship plumes.  
334 The transect-based sampling approach provides researchers with a relatively simple method of capturing data inside the  
335 plume. The principal flaws with this method are that there is no guarantee that the plume will be captured during a transect,  
336 and the degree to which the UAV enters the plume can vary between transects. A potential answer to these issues is a non-  
337 transect based approach in which the UAV system is made to hover inside the plume for a given period of time, ensuring  
338 data is collected. This also allows for the collection of many more data points inside the plume, ensuring accurate and  
339 repeatable data. Despite these advantages this method has proven to be challenging as it is difficult to verify whether the  
340 UAV is within the plume, when it is not visible to the naked eye especially in variable wind conditions. A potential solution  
341 is the implementation of sensors and instrumentation which transmit data to the ground station in real time. Using this data  
342 as a feedback mechanism, it would be possible to orient the UAV position so it hovers within the plume, ensuring that more  
343 accurate and repeatable data is collected on every flight.

#### 344 Acknowledgements

345 The authors would like to acknowledge the ARCAA Operations Team (Dirk Lessner, Gavin Broadbent) who operated the  
346 Unmanned Aerial Vehicle (S800). This research was supported by the Australian Research Council Discovery Grant  
347 DP150101649 and the Marine National Facility. The authors would like to thank the Captain and the crew of the RV  
348 Investigator as well as the on board MNF support staff as without their support and effort this research would not have been  
349 possible.

#### 350 Reference

351 NPRM 1309OS - Remotely Piloted Aircraft Systems.  
352 Agrawal, H.; Malloy, Q.G.J.; Welch, W.A.; Wayne Miller, J.; Cocker Iii, D.R. In-use gaseous and particulate matter emissions from a  
353 modern ocean going container vessel. *Atmospheric Environment* 2008;42:5504-5510  
354 Alföldy, B.; Lööv, J.B.; Lagler, F.; Mellqvist, J.; Berg, N.; Beecken, J.; Weststrate, H.; Duyzer, J.; Bencs, L.; Horemans, B.; Cavalli, F.;  
355 Putaud, J.P.; Janssens-Maenhout, G.; Csordás, A.P.; Van Grieken, R.; Borowiak, A.; Hjorth, J. Measurements of air pollution  
356 emission factors for marine transportation in SECA. *Atmos Meas Tech* 2013;6:1777-1791  
357 Anderson, M.; Salo, K.; Hallquist, Å.M.; Fridell, E. Characterization of particles from a marine engine operating at low loads.  
358 *Atmospheric Environment* 2015;101:65-71  
359 Balzani Lööv, J.M.; Alföldy, B.; Gast, L.F.L.; Hjorth, J.; Lagler, F.; Mellqvist, J.; Beecken, J.; Berg, N.; Duyzer, J.; Weststrate, H.; Swart,  
360 D.P.J.; Berkhouit, A.J.C.; Jalkanen, J.P.; Prata, A.J.; Van Der Hoff, G.R.; Borowiak, A. Field test of available methods to  
361 measure remotely SO<sub>x</sub> and NO<sub>x</sub> emissions from ships. *Atmospheric Measurement Techniques* 2014;7:2597-2613  
362 Beecken, J.; Mellqvist, J.; Salo, K.; Ekholm, J.; Jalkanen, J.P. Airborne emission measurements of SO<sub>2</sub>, NO<sub>x</sub> and particles from  
363 individual ships using a sniffer technique. *Atmospheric Measurement Techniques* 2014a;7:1957-1968  
364 Beecken, J.; Mellqvist, J.; Salo, K.; Ekholm, J.; Jalkanen, J.P. Airborne emission measurements of SO<sub>2</sub>, NO<sub>x</sub> and particles from  
365 individual ships using a sniffer technique. *Atmos Meas Tech* 2014b;7:1957-1968  
366 Berg, N.; Mellqvist, J.; Jalkanen, J.P.; Balzani, J. Ship emissions of SO<sub>2</sub> and NO<sub>2</sub>: DOAS measurements from airborne platforms.  
367 *Atmospheric Measurement Techniques* 2012;5:1085-1098  
368 Blasco, J.; Duran-Grados, V.; Hampel, M.; Moreno-Gutierrez, J. Towards an integrated environmental risk assessment of emissions from  
369 ships' propulsion systems. *Environment international* 2014;66:44-47  
370 Brady, J.M.; Stokes, M.D.; Bonnardel, J.; Bertram, T.H. Characterization of a Quadrotor Unmanned Aircraft System for Aerosol-Particle-  
371 Concentration Measurements. *Environmental Science & Technology* 2016;50:1376-1383



372 Cappa, C.D.; Williams, E.J.; Lack, D.A.; Buffaloe, G.M.; Coffman, D.; Hayden, K.L.; Herndon, S.C.; Lerner, B.M.; Li, S.M.; Massoli, P.;  
373 McLaren, R.; Nuaaman, I.; Onasch, T.B.; Quinn, P.K. A case study into the measurement of ship emissions from plume  
374 intercepts of the NOAA ship Miller Freeman. *Atmos Chem Phys* 2014;14:1337-1352

375 Chen, G.; Huey, L.G.; Trainer, M.; Nicks, D.; Corbett, J.; Ryerson, T.; Parrish, D.; Neuman, J.A.; Nowak, J.; Tanner, D.; Holloway, J.;  
376 Brock, C.; Crawford, J.; Olson, J.R.; Sullivan, A.; Weber, R.; Schaufler, S.; Donnelly, S.; Atlas, E.; Roberts, J.; Flocke, F.;  
377 Hübner, G.; Fehsenfeld, F. An investigation of the chemistry of ship emission plumes during ITCT 2002. *Journal of Geophysical  
378 Research: Atmospheres* 2005;110:D10S90

379 Cooper, D.A. Exhaust emissions from high speed passenger ferries. *Atmospheric Environment* 2001;35:4189-4200

380 Cooper, D.A. HCB, PCB, PCDD and PCDF emissions from ships. *Atmospheric Environment* 2005;39:4901-4912

381 Corbett, J.J.; Farrell, A. Mitigating air pollution impacts of passenger ferries. *Transportation Research Part D: Transport and Environment*  
382 2002;7:197-211

383 Corbett, J.J.; Koehler, H.W. Updated emissions from ocean shipping. *Journal of Geophysical Research: Atmospheres* 2003;108:4650

384 Corbett, J.J.; Winebrake, J.J.; Green, E.H.; Kasibhatla, P.; Eyring, V.; Lauer, A. Mortality from Ship Emissions: A Global Assessment.  
385 *Environmental Science & Technology* 2007a;41:8512-8518

386 Corbett, J.J.; Winebrake, J.J.; Green, E.H.; Kasibhatla, P.; Eyring, V.; Lauer, A. Mortality from Ship Emissions: A Global Assessment.  
387 *Environmental Science & Technology* 2007b;41:8512-8518

388 DJI. DJI S800-evo. 2014

389 Eyring, V.; Köhler, H.W.; van Aardenne, J.; Lauer, A. Emissions from international shipping: 1. The last 50 years. *Journal of Geophysical  
390 Research: Atmospheres* 2005;110:D17305

391 Fierz, M.; Burtscher, H.; Steigmeier, P.; Kasper, M. Field measurement of particle size and number concentration with the Diffusion Size  
392 Classifier (DiSC). *SAE Technical Paper*; 2008

393 Fuglestvedt, J.; Berntsen, T.; Eyring, V.; Isaksen, I.; Lee, D.S.; Sausen, R. Shipping Emissions: From Cooling to Warming of Climate—  
394 and Reducing Impacts on Health. *Environmental Science & Technology* 2009;43:9057-9062

395 Gonzalez, F.; Castro, M.P.G.; Narayan, P.; Walker, R.; Zeller, L. Development of an autonomous unmanned aerial system to collect time-  
396 stamped samples from the atmosphere and localize potential pathogen sources. *Journal of Field Robotics* 2011;28:961-976

397 Hak, C.S.; Hallquist, M.; Ljungström, E.; Svane, M.; Pettersson, J.B.C. A new approach to in-situ determination of roadside particle  
398 emission factors of individual vehicles under conventional driving conditions. *Atmospheric Environment* 2009;43:2481-2488

399 Hallquist, Å.M.; Fridell, E.; Westerlund, J.; Hallquist, M. Onboard Measurements of Nanoparticles from a SCR-Equipped Marine Diesel  
400 Engine. *Environmental Science & Technology* 2013a;47:773-780

401 Hallquist, Å.M.; Fridell, E.; Westerlund, J.; Hallquist, M. Onboard Measurements of Nanoparticles from a SCR-Equipped Marine Diesel  
402 Engine. *Environmental Science & Technology* 2013b;47:773-780

403 Hobbs, P.V.; Garrett, T.J.; Ferek, R.J.; Strader, S.R.; Hegg, D.A.; Frick, G.M.; Hoppel, W.A.; Gasparovic, R.F.; Russell, L.M.; Johnson,  
404 D.W. Emissions from ships with respect to their effects on clouds. *Journal of the atmospheric sciences* 2000;57:2570-2590

405 Inc., P. Picarro G2401 Analyzer. 2017

406 Isakson, J.; Persson, T.A.; Selin Lindgren, E. Identification and assessment of ship emissions and their effects in the harbour of Göteborg,  
407 Sweden. *Atmospheric Environment* 2001;35:3659-3666

408 Jayaratne, E.R.; Ristovski, Z.D.; Meyer, N.; Morawska, L. Particle and gaseous emissions from compressed natural gas and ultralow  
409 sulphur diesel-fuelled buses at four steady engine loads. *Science of The Total Environment* 2009;407:2845-2852

410 Jonsson, Å.M.; Westerlund, J.; Hallquist, M. Size-resolved particle emission factors for individual ships. *Geophysical Research Letters*  
411 2011;38:n/a-n/a

412 Juwono, A.M.; Johnson, G.R.; Mazaheri, M.; Morawska, L.; Roux, F.; Kitchen, B. Investigation of the airborne submicrometer particles  
413 emitted by dredging vessels using a plume capture method. *Atmospheric Environment* 2013;73:112-123

414 Kasper, A.; Aufdenblatten, S.; Forss, A.; Mohr, M.; Burtscher, H. Particulate Emissions from a Low-Speed Marine Diesel Engine. *Aerosol  
415 Science and Technology* 2007;41:24-32

416 Lack, D.; Lerner, B.; Granier, C.; Baynard, T.; Lovejoy, E.; Massoli, P.; Ravishankara, A.R.; Williams, E. Light absorbing carbon  
417 emissions from commercial shipping. *Geophysical Research Letters* 2008;35:L13815

418 Lack, D.A.; Cappa, C.D.; Langridge, J.; Bahreini, R.; Buffaloe, G.; Brock, C.; Cerully, K.; Coffman, D.; Hayden, K.; Holloway, J.; Lerner,  
419 B.; Massoli, P.; Li, S.-M.; McLaren, R.; Middlebrook, A.M.; Moore, R.; Nenes, A.; Nuaaman, I.; Onasch, T.B.; Peischl, J.;  
420 Perring, A.; Quinn, P.K.; Ryerson, T.; Schwartz, J.P.; Spackman, R.; Wofsy, S.C.; Worsnop, D.; Xiang, B.; Williams, E. Impact  
421 of Fuel Quality Regulation and Speed Reductions on Shipping Emissions: Implications for Climate and Air Quality.  
422 *Environmental Science & Technology* 2011;45:9052-9060

423 Lack, D.A.; Corbett, J.J.; Onasch, T.; Lerner, B.; Massoli, P.; Quinn, P.K.; Bates, T.S.; Covert, D.S.; Coffman, D.; Sierau, B.; Herndon, S.;  
424 Allan, J.; Baynard, T.; Lovejoy, E.; Ravishankara, A.R.; Williams, E. Particulate emissions from commercial shipping:  
425 Chemical, physical, and optical properties. *Journal of Geophysical Research: Atmospheres* 2009;114:D00F04

426 Malaver Rojas, J.A.; González, L.F.; Motta, N.; Villa, T.F.; Etse, V.K.; Puig, E. Design and flight testing of an integrated solar powered  
427 UAV and WSN for greenhouse gas monitoring emissions in agricultural farms. 2015 IEEE/RSJ International Conference on  
428 Intelligent Robots and Systems: IEEE; 2015

429 Mazaheri, M.; Johnson, G.R.; Morawska, L. Particle and Gaseous Emissions from Commercial Aircraft at Each Stage of the Landing and  
430 Takeoff Cycle. *Environmental Science & Technology* 2009;43:441-446

431 Mueller, L.; Jakobi, G.; Czech, H.; Stengel, B.; Orasche, J.; Arteaga-Salas, J.M.; Karg, E.; Elsasser, M.; Sippula, O.; Streibel, T.; Slowik,  
432 J.G.; Prevot, A.S.H.; Jokiniemi, J.; Rabe, R.; Harndorf, H.; Michalke, B.; Schnelle-Kreis, J.; Zimmermann, R. Characteristics  
433 and temporal evolution of particulate emissions from a ship diesel engine. *Applied Energy* 2015;155:204-217

434 Murphy, S.; Agrawal, H.; Sorooshian, A.; Padró, L.T.; Gates, H.; Hersey, S.; Welch, W.A.; Jung, H.; Miller, J.W.; Cocker III, D.R.;  
435 Nenes, A.; Jonsson, H.H.; Flagan, R.C.; Seinfeld, J.H. Comprehensive simultaneous shipboard and airborne characterization of  
436 exhaust from a modern container ship at sea. *Environ Sci Technol* 2009;43:4626-4640

437 Petzold, A.; Hasselbach, J.; Lauer, P.; Baumann, R.; Franke, K.; Gurk, C.; Schlager, H.; Weingartner, E. Experimental studies on particle  
438 emissions from cruising ship, their characteristic properties, transformation and atmospheric lifetime in the marine boundary  
439 layer. *Atmospheric Chemistry and Physics* 2008;8:2387-2403

440 Petzold, A.; Weingartner, E.; Hasselbach, J.; Lauer, P.; Kurok, C.; Fleischer, F. Physical properties, chemical composition, and cloud  
441 forming potential of particulate emissions from a marine diesel engine at various load conditions. *Environ Sci Technol*  
442 2010;44:3800-3805



443 Pirjola, L.; Pajunoja, A.; Walden, J.; Jalkanen, J.P.; Rönkkö, T.; Kousa, A.; Koskentalo, T. Mobile measurements of ship emissions in two  
444 harbour areas in Finland. *Atmospheric Measurement Techniques* 2014a;7:149-161  
445 Pirjola, L.; Pajunoja, A.; Walden, J.; Jalkanen, J.P.; Rönkkö, T.; Kousa, A.; Koskentalo, T. Mobile measurements of ship emissions in two  
446 harbour areas in Finland. *Atmos Meas Tech* 2014b;7:149-161  
447 Reda, A.A.; Schnelle-Kreis, J.; Orasche, J.; Abbaszade, G.; Lintelmann, J.; Arteaga-Salas, J.M.; Stengel, B.; Rabe, R.; Harndorf, H.;  
448 Sippula, O.; Streibel, T.; Zimmermann, R. Gas phase carbonyl compounds in ship emissions: Differences between diesel fuel  
449 and heavy fuel oil operation. *Atmospheric Environment* 2015;112:370-380  
450 Ristovski, Z.D.; Miljevic, B.; Surawski, N.C.; Morawska, L.; Fong, K.M.; Goh, F.; Yang, I.A. Respiratory health effects of diesel  
451 particulate matter. *Respirology* 2012;17:201-212  
452 Schreier, S.F.; Peters, E.; Richter, A.; Lampel, J.; Wittrock, F.; Burrows, J.P. Ship-based MAX-DOAS measurements of tropospheric NO<sub>2</sub>  
453 and SO<sub>2</sub> in the South China and Sulu Sea. *Atmospheric Environment* 2015;102:331-343  
454 Sinha, P.; Hobbs, P.V.; Yokelson, R.J.; Christian, T.J.; Kirchstetter, T.W.; Bruijntjes, R. Emissions of trace gases and particles from two  
455 ships in the southern Atlantic Ocean. *Atmospheric Environment* 2003;37:2139-2148  
456 Streets, D.G.; Carmichael, G.R.; Arndt, R.L. Sulfur dioxide emissions and sulfur deposition from international shipping in Asian waters.  
457 *Atmospheric Environment* 1997;31:1573-1582  
458 UNCTAD. Review of Maritime Transport 2015. United Nations Conference on Trade and Development UNCTAD 2015;  
459 USEPA-OTAC. USEPA-OTAC, 2012. <http://www.epa.gov/otaq/oceanvessels.htm#regs>, Ocean Vessels and Large Ships. US  
460 Environmental Protection Agency, Office-of-Transportation-and-Air-Quality. . 2012;  
461 Viana, M.; Hammingh, P.; Colette, A.; Querol, X.; Degraeuwe, B.; Vlieger, I.d.; Van Aardenne, J. Impact of maritime transport emissions  
462 on coastal air quality in Europe. *Atmospheric Environment* 2014;90:96-105  
463 Westerlund, J.; Hallquist, M.; Hallquist, Å.M. Characterization of fleet emissions from ships through multi-individual determination of  
464 size-resolved particle emissions in a coastal area. *Atmospheric Environment* 2015;112:159-166  
465 WHO. Review of evidence on health aspects of air pollution 2013  
466 Williams, E.J.; Lerner, B.M.; Murphy, P.C.; Herndon, S.C.; Zahniser, M.S. Emissions of NO<sub>x</sub>, SO<sub>2</sub>, CO, and HCHO from commercial  
467 marine shipping during Texas Air Quality Study (TexAQS) 2006. *Journal of Geophysical Research: Atmospheres*  
468 2009;114:D21306  
469 Winnes, H.; Moldanova, J.; Anderson, M.; Fridell, E. On-board measurements of particle emissions from marine engines using fuels with  
470 different sulphur content. *Proc Inst Mech Eng Part M J Eng Marit Environ* 2016;230:45-54  
471

472